

Article

Use of Combined Observational- and Model-Derived Photochemical Indicators to Assess the O₃-NO_x-VOC System Sensitivity in Urban Areas

Edson R. Carrillo-Torres, Iván Y. Hernández-Paniagua and Alberto Mendoza *

School of Engineering and Sciences, Tecnológico de Monterrey, Av. Eugenio Garza Sada 2501, Monterrey, NL 64849, Mexico; edson.carrillotr@gmail.com (E.R.C.-T.); iyassmany@itesm.mx (I.Y.H.-P.)

* Correspondence: mendoza.alberto@itesm.mx; Tel.: +52-81-8158-2091

Academic Editor: Bernhard Rappenglueck

Received: 10 December 2016; Accepted: 20 January 2017; Published: 26 January 2017

Abstract: Tropospheric levels of O₃ have historically exceeded the official annual Mexican standards within the Monterrey Metropolitan Area (MMA) in NE Mexico. High-frequency and high-precision measurements of tropospheric O₃, NO_y, NO₂, NO, CO, SO₂, PM₁₀ and PM_{2.5} were made at the Obispadó monitoring site near the downtown MMA from September 2012 to August 2013. The seasonal cycles of O₃ and NO_y are driven by changes in meteorology and to a lesser extent by variations in primary emissions. The NO_y levels were positively correlated with O₃ precursors and inversely correlated with O₃ and wind speed. Recorded data were used to assess the O₃-Volatile Organic Compounds (VOC)-NO_x system's sensitivity through an observational-based approach. The photochemical indicator O₃/NO_y was derived from measured data during the enhanced O₃ production period (12:00–18:00 Central Daylight Time (CDT), GMT-0500). The O₃/NO_y ratios calculated for this time period showed that the O₃ production within the MMA is VOC sensitive. A box model simulation of production rates of HNO₃ (P_{HNO_3}) and total peroxides (P_{perox}) carried out for O₃ episodes in fall and spring confirmed the VOC sensitivity within the MMA environment. No significant differences were observed in O₃/NO_y from weekdays to weekends or for P_{HNO_3}/P_{perox} ratios, confirming the limiting role of VOCs in O₃ production within the MMA. The ratified photochemical regime observed may allow the environmental authorities to revise and verify the current policies for air quality control within the MMA.

Keywords: air quality; box model; NO_y; photochemistry; wind sector analysis

1. Introduction

Increased tropospheric levels of O₃ can be harmful for human health, vegetation and built infrastructure [1–3]. In the troposphere, O₃ is produced by photochemical reactions between volatile organic compounds (VOCs) and nitrogen oxides (NO_x = NO + NO₂) in a non-linear O₃-VOC-NO_x system not fully unraveled yet [3]. Due to the non-linearity of the O₃-VOC-NO_x system, O₃ production can be VOC sensitive when controlled by the input of VOCs and increase in response to increased VOC emissions, but constant NO_x levels. Conversely, O₃ production can be NO_x-sensitive when NO_x emissions govern the system, and O₃ mixing ratios increase in response to increased NO_x emissions, but remain constant to variations of VOCs [4–6]. Typical VOC/NO_x ratios for VOC-sensitive regimes are <4, while those for NO_x-sensitive regimes are >15 [5]. However, existing studies report changes in O₃ production during the daytime and from weekdays to weekends from VOC- to NO_x-sensitive regimes and vice versa within the same region as a result of changes in the emissions of precursors and meteorology [7–11]. Because the majority of existing policies to reduce the tropospheric levels of O₃ within urban areas focus on reducing the emissions of precursors, their success depends

strongly on untangling, with accuracy, the sensitivity of O₃ production. The sensitivity of the O₃ production system has been traditionally assessed using either photochemical box models or 3D chemistry/transport models to predict changes under different control scenarios of VOCs and NO_x emissions or observational-based approaches (Table 1). Models are run frequently with recorded data for ambient air pollutants as input to infer the processes that govern the O₃ production. However, the accuracy of the results generated by emissions-driven models also depends on multiple assumptions in the input data (including the emission rates), which can be highly uncertain and could lead to contradictory results [5]. It has also been reported that different modeling systems applied to the same air basin can yield different results [12,13]. In addition, as exemplified in Table 1, modeling studies tend to cover short-term episodes, given the amount of resources needed to model large periods of time. Thus, an effort has to be made to choose modeling episodes that are representative of the phenomena being addressed.

Table 1. Summary of previous assessments of the O₃ production sensitivity system using photochemical indicators.

Reference	Location	Altitude (m a.s.l.)	Methodology	Chemical Species	Period	Photochemical Regime
[14]	Baden-Württemberg and Berlin-Brandenburg, Germany; Po Valley, Italy	~245; ~34	Modeling	O ₃ , H ₂ O ₂ , HNO ₃ , NO _x , VOC, and NO _y	May 1998	Berlin-Brandenburg and Po Valley: VOC-sensitive. Baden-Württemberg: NO _x sensitive
[15]	Seoul and Gyeonggi, Korea	44	Observations	NO _x , NO _y , H ₂ O ₂ , O ₃ , CO, HCHO, and PAN *	1 May–30 June 2004; 15 May–17 June 2004	VOC sensitive
[16]	Tokyo, Japan	37	Observations	NO _y and NO _y , and PM ₁₀	24 July–13 August 2003; 1–15 October 2003	NO _x -sensitive regime during 12–14 August
[17]	Beijing, China	44	Observations	NO, NO _x , and NO _y	1 August–9 September 2006	VOC sensitive
[18]	Pingtung, Chao-Chou, Kenting, Taiwan	~17	Modeling and observations	H ₂ O ₂ , HNO ₃ , and NO _y	5-day period by season during 2003–2004	Pingtung, Chao-Chou: both regimes. Kenting: NO _x sensitive
[19]	Monterrey, México	540	Modeling	O ₃ and NO _y	22–27 August 2005	VOC sensitive

* Peroxyacetyl nitrate.

The observational methods to assess the O₃ production sensitivity based on datasets of robust measurements for involved species in the O₃-VOC-NO_x system represent a feasible alternative to the traditional modeling approach. One advantage of this approach over pure modeling studies is that larger time frames (several months or more worth of data) can be used (Table 1). Some of the typical photochemical indicators used in the observational approach are hydrogen peroxide (H₂O₂) [5,18,20], nitric acid (HNO₃) [5,18,20], total odd nitrogen (NO_y = NO + NO₂ + peroxyacetyl nitrate (PAN) + HNO₃ + other inorganic and organic nitrates) [12,21,22] and the O₃/NO_y ratio [23–25]. For example, from a numerical assessment conducted for six polluted regions in the U.S., O₃/NO_y ratios ≤ 6 and ≥ 8 were determined for VOC- and NO_x-sensitive regimes, respectively, when mixing ratios of O₃ are >100 ppb; and O₃/NO_y ratios ≤ 11 and ≥ 15 in VOC- and NO_x-sensitive conditions, respectively, in environments of O₃ mixing ratios < 80 ppb [25]. In Southern Taiwan, two VOC-sensitive urban areas with O₃/NO_y ratios < 6 and one NO_x-sensitive area with O₃/NO_y ratios > 7 were observed during 2003–2004 [18]. O₃/NO_y average ratios of 5.1 ± 3.2 and 13.6 ± 4.7 for VOC- and partially NO_x-sensitive O₃ production, respectively, at two sites in Valencia, Spain, were observed during 2010–2011 [26]. The observed variations in the O₃/NO_y ratios both for VOC- and NO_x-sensitive regimes arise from different behaviors of the indicator relative to the environmental conditions (clean, moderately polluted or highly polluted environments) [25].

The photochemical indicators that have been used arise from the analysis of the main reaction pathways of the O₃-VOC-NO_x system. In a simplified manner, the initial steps of the oxidation of VOCs in the atmosphere can be represented by the following reactions [25]:



(where R is a general hydrocarbons chain)



(where R' is an intermediate VOC)



O₃ accumulates in the atmosphere as NO is transformed to NO₂ (through Reaction 2) without destroying O₃; i.e., as the NO + O₃ → NO₂ + O₂ reaction becomes less relevant because of the presence of VOCs that provide a source of odd hydrogen radicals that foster other reactions. Thus, the prevalence of a given photochemical regime is driven by the chemistry of hydrogen radicals. For example, it has been shown that the chain terminating steps that involve the formation of peroxides (Reactions 5 and 6) and nitric acid (Reaction 7) compete as radical sinks, and if peroxides dominate, then a NO_x-sensitive condition will occur [5,25]. Similar theoretical arguments are provided to justify the use of NO_y as a photochemical indicator: the split between regimes can be established from the strength of odd nitrogen sources against odd hydrogen sources. Further details can be found elsewhere [5,25].

In Mexico City, a VOC-sensitive regime was determined for most of the urban area using the O₃/NO_y, O₃/NO_z and NO_y indicators derived from tropospheric measurements made at three monitoring sites within the city [12]. In addition, a numerical simulation carried out by a 3D photochemistry/transport model was used to estimate the transition values of the indicators between regimes for a two-week period in April 2004; the transition value was ~8.1, and the average O₃/NO_y at the studied site was 2.6. Besides Mexico City, other large metropolitan areas in the country also experience frequent O₃ episodes, although they have received relatively little attention. For instance, the Monterrey Metropolitan Area (MMA; Figure 1), which is the third-largest metropolitan area in Mexico, has historically experienced high levels of O₃, PM₁₀ and PM_{2.5}. Official reports show that within the MMA, breaches of the 1 h 110 ppb and running 8 h 80 ppb O₃ official Mexican standards (Norma Oficial Mexicana or NOM, in Spanish) were frequent during 2000–2013 [27].

At the Obispado monitoring site (OBI) located near the downtown area of Monterrey (Figure 1), the O₃ 1 h NOM was exceeded annually between two and 17 times during 2000–2013, whereas the O₃ running 8 h NOM was breached between four and 38 times during the same period. Furthermore, an increase in the frequency of breaches of both the O₃ 1 h average and the O₃ running 8 h average is expected due to the introduction of lower standard values of 95 and 70 ppb, respectively, applicable since October 2014. This highlights the importance of untangling the O₃ production sensitivity system to introduce effective emission controls, which can lead to an improvement in the air quality within the MMA. To date, only one study has recently assessed the O₃ production sensitivity system within the MMA [19]; a VOC-sensitive regime was observed based on numerical simulations performed with the Community Multi-scale Air Quality (CMAQ) model. However, those results come from a six-day

O₃ episode during summer 2005, which may not be representative of the environmental conditions prevailing the rest of the year [19].

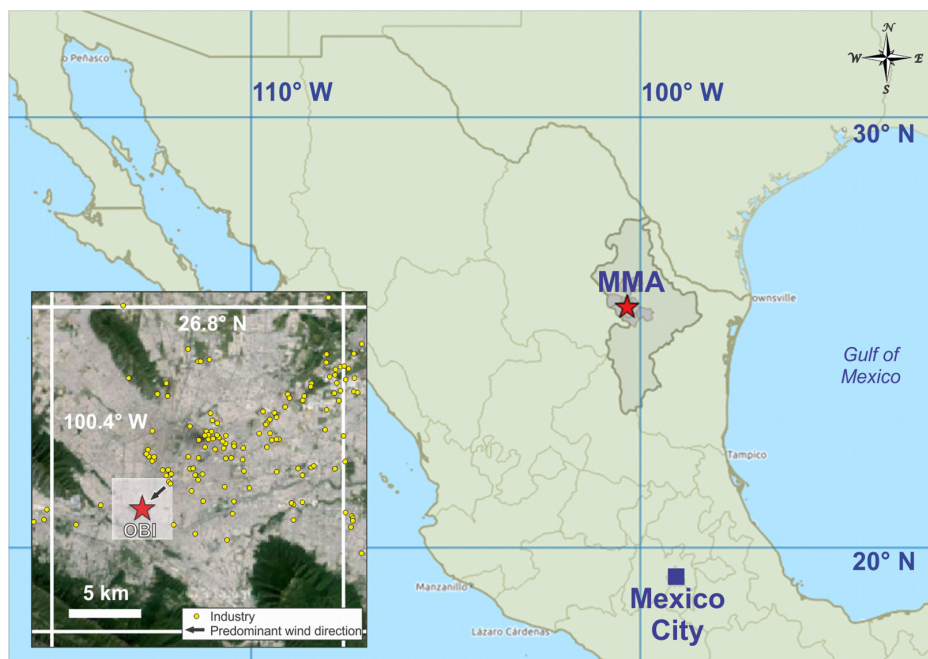


Figure 1. The Monterrey Metropolitan Area (MMA) in the national context in northeast Mexico and the location of the Obispo (OBI) site within the MMA. The shadowed white square surrounding the OBI site represents the 4 km × 4 km domain used for modeling purposes.

This study presents the assessment of the O₃ photochemical production regime within the MMA over a one-year period carried out by combining box-modeling and observational approaches to analyze the behavior of two photochemical indicators. The photochemical indicator O₃/NO_y was derived from recorded data within the MMA for tropospheric air pollutants from September 2012 to August 2013, which was used to analyze the O₃ production system. Ratios of the HNO₃ and total peroxide production rates (P_{HNO_3}/P_{perox}) were computed using a box-model and were subsequently employed to evaluate the results derived from the recorded ambient data. Additionally, the existence of a weekend effect in the O₃ production within the MMA was evaluated using the O₃/NO_y and P_{HNO_3}/P_{perox} ratios.

2. Methods

2.1. Study Site Description and Air Pollutant Monitoring

The MMA is located in northeast Mexico, some 230 km S of the United States border, and lies at an average altitude of 550 m a.s.l. (Figure 1). It is the third-most populous urban area in the country with around 5.12 million inhabitants and the second-largest industrial region [28]. The MMA also has the highest vehicle motorization index in Mexico of around 0.5 vehicles per inhabitant. Continuous measurements of typical criteria air pollutants (O₃, NO, NO₂, CO, SO₂ and PM₁₀) and meteorological parameters (wind speed (WS), wind direction (WD), relative humidity (RH), pressure, solar radiation (SR) and temperature) have been made since November 1992 at five monitoring sites that form part of the Integral Environmental Monitoring System (SIMA) of the Nuevo Leon Government. PM_{2.5} measurements began in 2003.

Additionally, NO_y measurements were conducted at the OBI site from July 2012 to August 2013 using a Thermo Scientific chemiluminescence analyzer 42i-Y, in accordance with the United States Environmental Protection Agency (EPA), RFNA-1289-074. The OBI site location near the MMA

downtown (25°40'33" N, 100°20'18" W; Figure 1) is ideal to record emissions from the industrial, domestic and mobile sources depending on air masses' trajectories. Table 2 shows the instrumentation used to measure air pollutants and meteorological parameters at OBI. Calibration and maintenance procedures were carried out according to official protocols established in the Mexican standards NOM-036-SEMARNAT-1993 and NOM-156-SEMARNAT-2012.

Table 2. Instrumentation used to measure air pollutants and meteorological parameters during July 2012–August 2013 at the Obispo (OBI) site. WS, wind speed; WD, wind direction; SR, solar radiation.

Parameter	Instrument Model	Detector	EPA Equivalent Method Number	Stated Precision (±)
O ₃	Thermo Environmental 49C	UV photometry	EQOA-0880-047	1 ppb
NO-NO ₂ -NO _x	Thermo Environmental 42C	Chemiluminescence	RFNA-1289-074	0.4 ppb
NO-DIF-NO _y	Thermo Environmental 42i NO _y	Chemiluminescence	RFNA-1289-074	50 ppb
PM ₁₀	Met One BAM 1020	Beta attenuation	EQPM-0798-122	5 µg·m ⁻³
CO	Thermo Environmental 48C	Non-dispersive IR	RFCA-0981-054	1 ppm
SO ₂	Thermo Environmental 43C	Fluorescence	EQSA-0486-060	1 ppb
WS	Met One 010C	Anemometer	n.a.	1%
WD	Met One 020C	Potentiometer	n.a.	3°
Temperature	Met One 060A	Multi-stage thermistor	n.a.	0.5 °C
Pressure	Met One 090D	Barometric sensor	n.a.	1.35 mbar
RH	Met One 083E	Capacitance sensor	n.a.	2%
SR	Met One 095	Pyranometer	n.a.	1%

n.a.: not applicable.

2.2. Capture Rate and Seasonal and Wind Sector Analyses

Figure 2 shows the data capture of validated 1 h averages of air pollutants and meteorological data recorded at OBI from September 2012 to August 2013. Data capture for air pollutants and meteorological parameters ranged from 84.6% (SO₂) to 96.0% (CO) and from 96.0% (RH) to 98.8% (pressure), respectively. To perform seasonal analyses, 4 seasons were defined according to temperature records in the northern hemisphere: fall (September–November 2012), winter (December 2012–February 2013), spring (March–May 2013) and summer (June–August 2013). Wind-sector analyses were carried out by dividing the dataset into 8 wind sectors of 45° starting from 0° ± 22.5°. The lower bound of wind each sector was established by adding 0.5° to avoid the duplication of data.

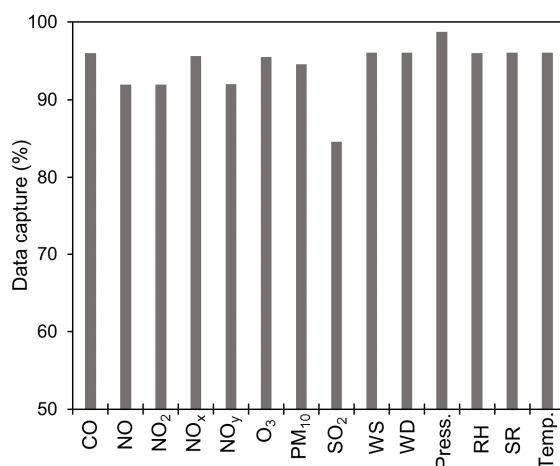


Figure 2. Data capture of 1 h averages for air pollutants and meteorological parameters recorded at the OBI site from September 2012 to August 2013.

2.3. Meteorology at the MMA

The climate at the MMA is semi-arid, with an annual average temperature of around 23 °C. Figure 3a shows that at OBI, the monthly temperature averages in summer are higher than 25 °C,

whereas temperatures in winter are typically below 20 °C. Similarly, the SR exhibits the highest monthly averages in summer and the lowest ones by late fall-early winter. The RH varies drastically during the year, with the lowest and highest averages typically observed in spring and fall, respectively. The rainfall within the MMA is frequent by late summer-early fall and scarce in the winter [29].

Figure 3b shows the frequency of the counts of WD occurrence at OBI by season from September 2012 to August 2013. Overall, the predominant WD is NE with frequencies of 34%–38% in spring and summer, respectively, although in winter, the greatest frequency of around 26% is observed for the E sector. Calm conditions (1 h averages) with a WS of less than 0.36 km·h⁻¹ occurred <1% of the time. A high WS (>15 km·h⁻¹) is typically observed in spring and summer for the E sector with frequencies >2% of the time. By contrast, a WS < 3 km·h⁻¹ shows the highest frequency in winter, mostly for the W and SW sectors.

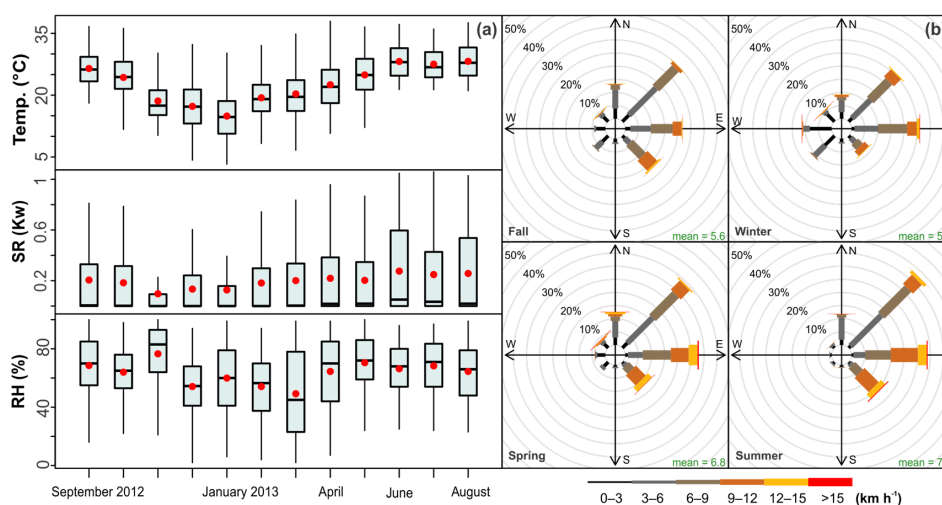


Figure 3. (a) Annual profile of the temperature, solar radiation (SR) and relative humidity (RH); (b) frequency of the counts of recorded wind direction occurrences at the OBI site during September 2012–August 2013. The horizontal black line shows monthly medians, and the red dots show monthly averages.

2.4. Statistical Analyses

To have a better understanding of the O₃/NO_y photochemical indicator data obtained here, statistical tests were performed to analyze and interpret the observed pollutants' dynamics. Descriptive statistics and seasonal profiles of data recorded at OBI from September 2012 to August 2013 were calculated using the openair package [30] for R software [31]. Correlations among air pollutants and meteorological data recorded were tested using a multiple linear regression analysis. A principal component analysis (PCA) was carried out to isolate the variables that govern the O₃ production within the MMA. The variables identified as drivers of the O₃ production were subject to a cluster analysis (CA) to select daytime periods of enhanced photochemical activity. O₃/NO_y ratios calculated for the selected photochemical periods were analyzed by season, and a wind sector analysis was carried out to identify spatial variations in the photochemical processing of air masses arriving at OBI during September 2012–August 2013. Finally, the presence of a weekend effect in the diurnal production of O₃ was tested using an ANOVA analysis for O₃/NO_y ratios during the enhanced photochemical activity period. Data correlations, PCA, CA and ANOVA were carried out using IBM SPSS Statistics software v.19.0 (IBM, Armonk, NY, USA) for Windows.

2.5. Box Model Description and Simulations

Ratios of the HNO₃ and total peroxide production rates ($P_{\text{HNO}_3}/P_{\text{perox}}$) during high photochemical activity periods can be used to assess the O₃ production regime [25]. For example, typical VOC-sensitive

regimes exhibit P_{HNO_3}/P_{perox} ratios > 2 . For periods of enhanced photochemical activity within the MMA from September 2012 to August 2013, P_{HNO_3} and P_{perox} were calculated using the California/Carnegie Institute of Technology (CIT) 3D air quality model [32–34] in a box-model configuration [35]. Hourly-average P_{HNO_3}/P_{perox} ratios were calculated from the reaction rates constants estimated by the CIT model (i.e., the SAPRC90 photochemical mechanism [36]):

$$P_x = \sum_i k_i[A_i][B_i] - \sum_j k_j[C_j][x] \quad (8)$$

where P_x is the rate of the production of pollutant x and k_i and k_j are the reaction rate constants for the corresponding production and consumption reactions, respectively. Thus, $\sum_i k_i[A_i][B_i]$ accounts for the production of chemical species x from all relevant reactions ($[A_i]$ and $[B_i]$ are the concentrations of the corresponding reactants in the i -th reaction). Similarly, $\sum_j k_j[C_j][x]$ accounts for the consumption of species x ($[C_j]$ is the concentration of the species that reacts with x in the j -th reaction, and $[x]$ is the concentration of x).

The model domain comprised a box of 16 km², centered at the OBI site (Figure 1). The model vertical structure is analogous to that used by Young et al. [35] to account for the evolution of the mixing layer, setting the top of the domain at 3100 m a.g.l. Emissions data were obtained from the National Emissions Inventory of Mexico 2005 (NEI) [37]. Emission rates for CO, NO_x, VOCs, SO_x and NH₃ were derived following the methodology reported by Mendoza and García [38] to obtain temporally-distributed and chemically-speciated emission rates. The chemical speciation profiles for NO_x and VOC emissions were obtained from the U.S. EPA SPECIATE database for sources of emissions included in the NEI [39]. Meteorology inputs (temperature, humidity, WS and WD, SR and mixing layer height) were derived from 1-h average data recorded at the OBI site. SIMA 1-h averages of CO, NO, NO₂, O₃ and SO₂, together with 4-h average diurnal data for reactive hydrocarbons (RHCs), ketone, formaldehyde, acetaldehyde and isoprene data were used to constrain the model. The average RHC and individual VOC species data were obtained during sampling campaigns carried out within the MMA in the spring and fall of 2011 and 2012 [40,41]. Additionally, the CIT model was modified to include speciated NO_z (NO_y–NO_x) data in the initial conditions, which was calculated from NO_x and NO_y measurements made at the OBI site. NO_z was speciated using the average contributions of the 3 main species that typically form most of the NO_z produced in urban centers: 55% HNO₃, 40% PAN and 5% nitrous acid (HONO) [42,43].

Table 3 shows the modeled periods, which were chosen because the O₃ levels breached the 110 ppb 1 h NOM applicable during 2012–2013. The modeled periods include weekends and weekdays in the fall and spring, when O₃ typically exceeds the official air quality standards.

Table 3. Selected time periods to assess the O₃ production sensitivity using the California/Carnegie Institute of Technology (CIT) photochemical box model.

Period	Date	Season
1	1–8 September 2012	Fall
2	22–29 September 2012	Fall
3	6–13 March 2013	Spring
4	12–19 March 2013	Spring

3. Results and Discussion

3.1. Air Pollutants Annual Profiles

The recorded air pollutants exhibit an annual profile as a result of changes in precursor emissions and meteorology. Figure 4 shows the annual profile for O₃, NO_y, NO, NO₂ and CO recorded at the OBI site from September 2012 to August 2013. The O₃ exhibits the highest mixing ratios in spring 2013 as result of high photochemistry between NO_x and VOCs and the lowest ones in winter 2012 in antiphase

with NO_2 as a result of the reduced SR and low temperatures (Figure 3a). A downward spike in the O_3 mixing ratios is observed by mid-summer 2013, which is likely caused by a high WS typical of early summer. The decrease in O_3 during summer causes another peak in the annual cycle, which is observed by early fall. However, frequent rainfall leads to lower monthly averages of O_3 during fall than those in spring. The highest mixing ratios of NO_y are observed during winter as a result of the low SR and low temperature, which increase the NO_2 and NO build-up [23]. In contrast, the lowest mixing ratios of NO_y are observed during summer due to enhanced dispersion, large mixing height depths and high photochemical activity of O_3 precursors.

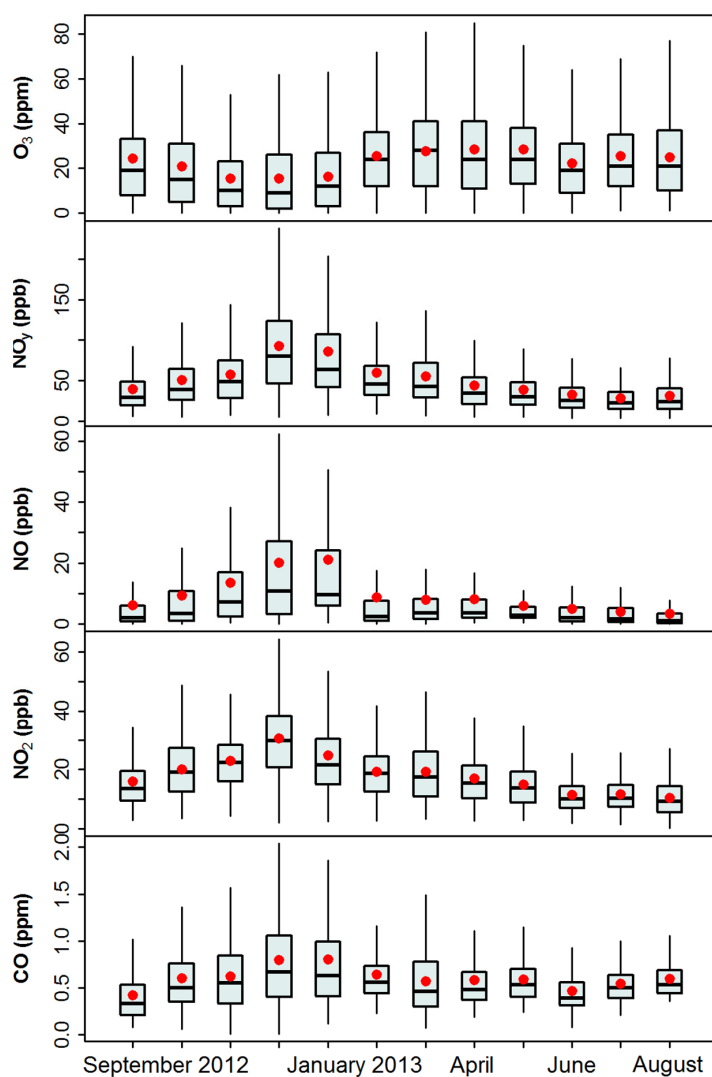


Figure 4. Annual profile of air pollutants recorded at the OBI site during September 2012 to August 2013. The horizontal black line shows monthly medians, and the red dots show monthly averages.

Table 4 shows the results of linear correlation analyses between NO_y and NO_2 , NO , O_3 , CO , SR, temperature and WS. A strong correlation between NO_2 and NO_y ($R = 0.819$) is observed in winter as a result of the low photolysis rates of NO_2 , which suggests that NO_2 is the main component of NO_y . Figure 5 shows the annual profiles of the $\text{NO}_y - \text{NO}$ difference and the NO_x/NO_y ratio. The $\text{NO}_y - \text{NO}$ difference exhibits the maxima and minima in winter and summer, respectively, which are in antiphase with the observed mixing ratios of O_3 from September 2012 to August 2013. In contrast, the NO_x/NO_y ratio exhibits the maxima by late fall-early winter and minima in early spring. The high values in the NO_x/NO_y ratio observed during winter confirm a build-up of NO_2 and NO , which implies that

NO_z is a low fraction of the total NO_y due to low photochemical processing [22]. During spring, low NO_x/NO_y ratios indicate an enhancement of the photochemical processing of the air masses, which could confirm the high O_3 mixing ratios observed in the season (Figure 4). The presumed high contribution of NO_z to NO_y during spring could also explain the weak correlation between NO_y and NO_2 ($R^2 < 0.411$) and between NO_y and NO ($R^2 < 0.275$) (Table 4). Finally, very weak correlations between NO_y and O_3 ($R^2 < 0.151$) are seen during the whole year due to their antiphase annual cycle, this is underlined during spring and summer when the photo-dissociation of NO_2 to produce O_3 is enhanced [44].

Table 4. Correlation coefficients (R^2) between NO_y and air pollutants and meteorological parameters recorded at the OBI site from September 2012 to August 2013.

Parameter	Fall 2012	Winter 2012	Spring 2013	Summer 2013
O_3 (ppb)	0.106	0.151	0.065	0.070
NO_2 (ppb)	0.676	0.819	0.411	0.783
NO (ppb)	0.610	0.661	0.275	0.615
CO (ppm)	0.420	0.664	0.227	0.712
Solar radiation ($\text{kW}\cdot\text{m}^{-2}$)	0.001 *	0.004	0.001 *	0.009
Temperature ($^{\circ}\text{C}$)	0.024	0.022	0.005	0.063
Wind speed ($\text{km}\cdot\text{h}^{-1}$)	0.247	0.203	0.112	0.225

* No significant correlation, $p > 0.05$.

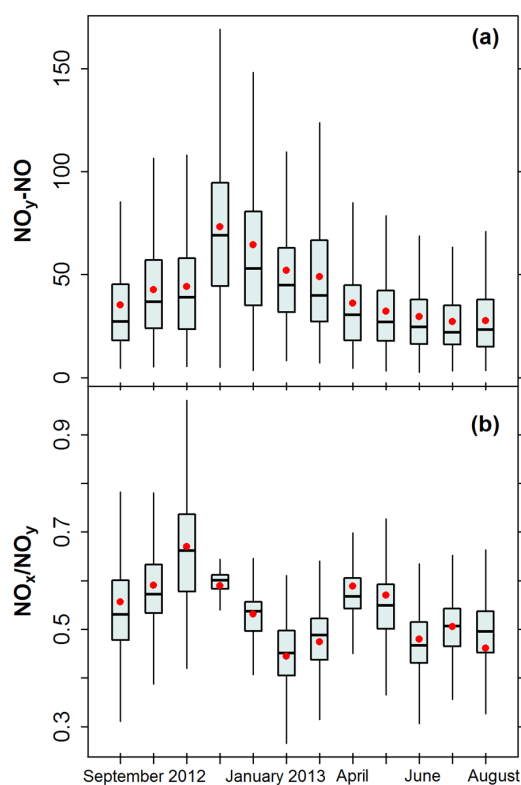


Figure 5. (a) Annual profile of the difference $\text{NO}_y - \text{NO}$ for data recorded at the OBI site from September 2012–August 2013; (b) NO_x/NO_y ratios during the same period. The horizontal black line shows monthly medians, and the red dots show monthly averages.

3.2. Wind Sector Analysis

Figure 6a shows pollution roses of the O_3 mixing ratios at OBI by WS. Overall, the mixing ratios of $\text{O}_3 > 50$ ppb are frequent in air masses arriving from the NE and E sectors at a $\text{WS} > 5 \text{ km}\cdot\text{h}^{-1}$ and

an increase in frequency at a $WS > 10 \text{ km}\cdot\text{h}^{-1}$, likely due to the local transport of O_3 and precursors from the upwind dense industrial area [40,45]. Similar to the MMA, an increase in the O_3 mixing ratios caused by upwind precursor emissions was observed at the Shangdianzi site near Beijing, China [22]. In that site, it was observed that large emissions of VOCs enhance the production of O_3 linked with an increase in the NO_z levels. Such an increase in NO_z levels ($>50 \text{ ppb}$) is also observed at OBI when the WS ranged from $1\text{--}5 \text{ km}\cdot\text{h}^{-1}$ for all wind sectors (Figure 6b), and for a $WS > 5 \text{ km}\cdot\text{h}^{-1}$ in air masses from the N-NE-E sectors, the location of major industrial sources of NO_x and VOC emissions.

In contrast, mixing ratios of $\text{O}_3 < 25 \text{ ppb}$ at OBI are typical during winter and show the highest frequency at a $WS < 1 \text{ km}\cdot\text{h}^{-1}$ and a reduced frequency at a $WS < 5 \text{ km}\cdot\text{h}^{-1}$ for all wind sectors, except for NE and E sectors. Similar to O_3 , the NO_z exhibits low mixing ratios ($<25 \text{ ppb}$) at a $WS > 10 \text{ km}\cdot\text{h}^{-1}$; however, at a low WS , mixing ratios of $\text{NO}_z > 50 \text{ ppb}$ are common for the SW and E sectors, which is likely due to the photochemical processing of NO_x emissions from mobile sources under stagnant conditions.

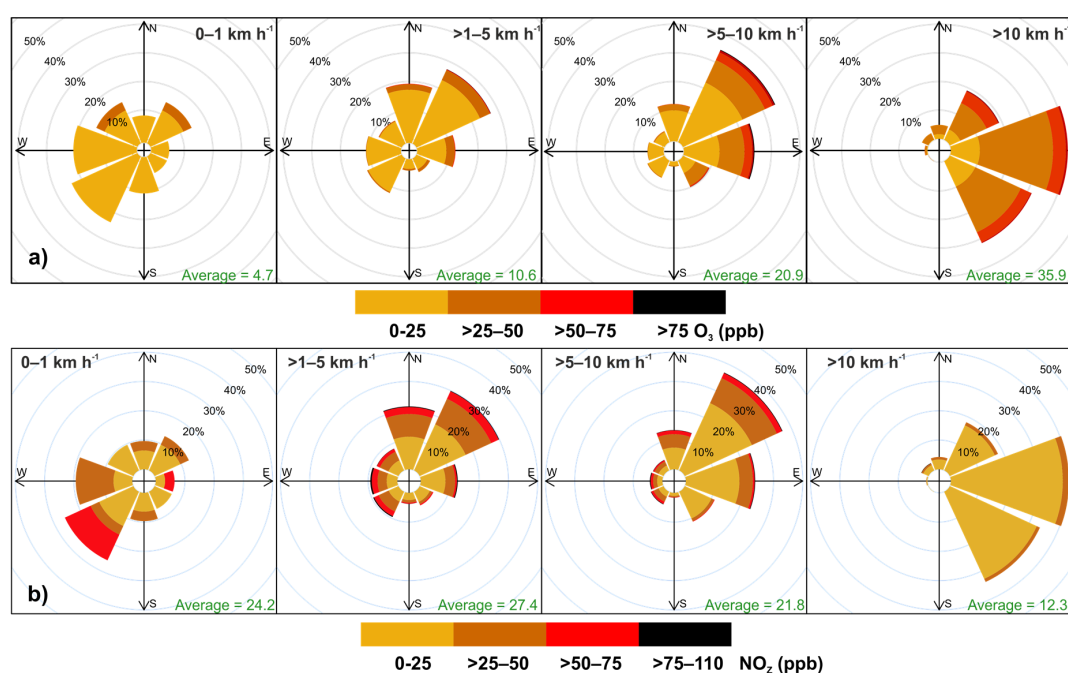


Figure 6. (a) Pollution roses of 1-h O_3 averages and (b) pollution roses of NO_z by wind speed (WS) recorded at the OBI site from September 2012–September 2013.

3.3. The Enhanced Photochemical Period

Photochemical indicators around the period of maximum photochemical activity for the chemical species involved in the O_3 production system may reflect daytime variations in photochemistry within the planetary boundary layer, and therefore, such indicators can be used to assess the photochemical regime of O_3 production [5,26]. For example, O_3/NO_y ratios were estimated from data recorded in the period of 13:00–17:00 Central Daylight Time (CDT, GMT-0500) during April 2004 at a downwind receptor site of photo-chemically-aged air masses within Mexico City [12]. Likewise, O_3/NO_y ratios from measurements made during 13:00–16:00 CET at two sampling sites in Valencia, Spain, during August 2010–May 2011 and May–October 2011 were calculated [26]. In the current study, the variables that govern the O_3 production within the MMA were isolated using a PCA for NO_y , NO_2 , NO , O_3 , CO , SO_2 , PM_{10} , $\text{PM}_{2.5}$ and temperature, WS , WD and SR data recorded from September 2012 to August 2013.

Table 5 shows that three components designated as PC1–3 are significant, which accounted for 67.2% of the total variability. The PC1 revealed a positive correlation among the precursors of O_3 ; NO_y ,

NO, NO₂ and CO. The PC2 correlates positively with O₃ and SR, which is explained by the photolysis of NO₂ during the daytime. The PC3 correlates positively with WD and temperature, which comprise the effect of the air mass origin and planetary boundary layer height that influences the dispersion of O₃. Dendrograms for the O₃ and SR data recorded within the MMA (PC2) were constructed to identify the hours of enhanced photochemistry, the period of maximum O₃ production. Figure 7 shows the annual average period of enhanced O₃ production from 12:00 to 18:00 CDT and O₃ depletion from 19:00 to 11:00, respectively.

Table 5. Results of the PCA performed using observations for air pollutants and meteorological data recorded at the OBI site from September 2012 to August 2013.

Component	PC1	PC2	PC3
NO _y	0.481	0.055	−0.009
NO ₂	0.387	0.087	−0.123
NO	0.375	0.029	0.151
O ₃	−0.226	0.447	0.075
CO	0.400	0.110	0.081
SO ₂	0.206	0.339	−0.348
PM ₁₀	0.230	0.354	−0.062
PM _{2.5}	0.261	0.234	0.129
SR	−0.090	0.497	0.031
Temperature	−0.197	0.370	0.411
WS	−0.288	0.276	0.084
WD	0.175	0.339	0.794
Cumulative variance (%)	39.5	59.5	67.2

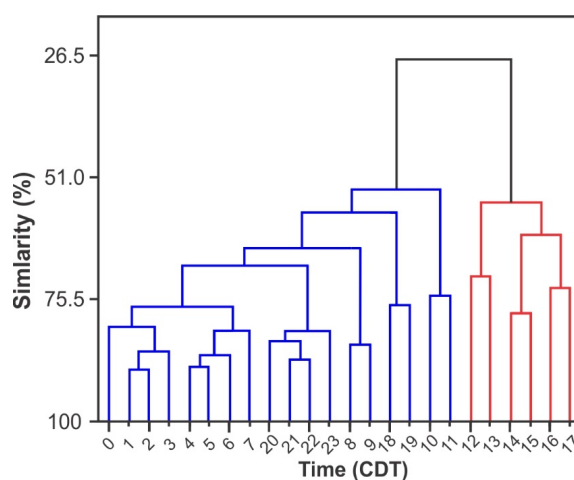


Figure 7. Dendrogram derived from the cluster analysis (CA) performed for 1-h averages of O₃ and SR data recorded at the OBI site from September 2012 to August 2013. The red cluster shows the period of enhanced photochemical activity.

3.4. Use of the O₃/NO_y Photochemical Indicator

The photochemical indicator O₃/NO_y was derived from measurements made during the period of 12:00–18:00 CDT at OBI during September 2012–August 2013. Figure 8 shows a box plot by season for O₃/NO_y ratios at OBI. Overall, the O₃/NO_y ratio ranged from 0.1 in fall 2012 to 4.8 in summer 2013, while medians and averages in O₃/NO_y ranged from 0.8 and from 0.9 in winter 2012 to 2.2 and to 2.3 in summer, respectively. The low O₃/NO_y ratios calculated at OBI during winter result from low O₃ levels and high NO_y levels, whereas the high O₃/NO_y ratios during summer derive from moderate O₃ levels, but low NO_y levels. The O₃/NO_y ratios observed in all seasons suggest that the O₃ production within the MMA is VOC sensitive throughout the entire year. This is in good agreement with prior results of O₃ production being VOC sensitive within the MMA based on

numerically-modeled O_3/NO_y ratios that ranged between 2.9 and when the highest 3.5 for the OBI site [19] and that are within the range of those calculated in the current study. The differences observed between the current and the referred prior results may arise from the fact that their modeled ratios were provided exclusively for 13:00 CDT and limited to a pollution episode in summer 2005.

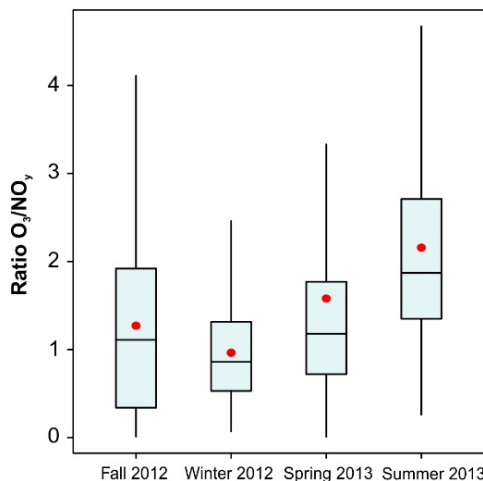


Figure 8. O_3/NO_y ratios by season derived from observations made at the OBI site during September 2012–August 2013. Ratios below six are typical of VOC-sensitive regimes.

The O_3/NO_y ratios calculated from 12:00 to 18:00 CDT at OBI were used to construct pollution roses by WS, which are shown in Figure 9. Overall, O_3/NO_y ratios < 2 are predominant at a $WS < 5 \text{ km}\cdot\text{h}^{-1}$ for all wind sectors and increased proportionally to WS, at a $WS > 5 \text{ km}\cdot\text{h}^{-1}$, although, this is only seen for the NE, E and SE sectors. The highest O_3/NO_y ratios observed (>4) were recorded in air masses arriving from the easterly sectors, NE-E-SE at a $WS > 5 \text{ km}\cdot\text{h}^{-1}$, and exhibit the highest frequency in line with the highest WS observed. Low O_3/NO_y ratios are typical in winter as result of low temperatures and low WS occurrence. A low WS may influence the formation and local transport of O_3 by limiting the horizontal and vertical mixing and the reactions of O_3 precursor emissions, which can also occur during other seasons. Moreover, at a low WS, the observed high values of NO_x/NO_y in Figure 5 suggest a low contribution of NO_z to NO_y , which is typical of low photochemical processing commonly seen in VOC-sensitive regimes [46]. By contrast, a high WS may enhance the photochemical processing of O_3 precursors and the transport of air masses travelling over rural areas located east of the MMA that typically have NO_x -sensitive regimes.

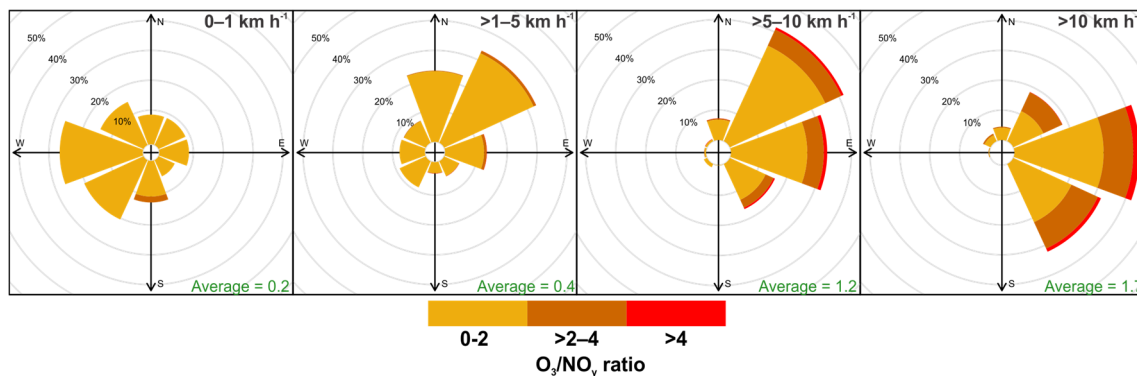


Figure 9. Pollution roses by WS of 1 h O_3/NO_y ratios calculated between 12:00 and 18:00 Central Daylight Time (CDT, GMT-0500) at the OBI site from September 2012 to August 2013.

No weekend effect (significant differences, $p > 0.05$) was observed in the O_3 mixing ratios and O_3/NO_y ratios between weekdays and weekends of all seasons (Table 6; Figure 10), despite the lower average O_3/NO_y ratios during weekdays. This lack of a weekend effect in the O_3 mixing ratios and the average O_3/NO_y ratios arise from the limiting role of VOCs in the weekday O_3 production, while reduced vehicular NO_x emissions during weekends increase the VOC/NO_y emission during weekends [47,48]. This decrease has counteracting effects on the O_3 production leading to similar O_3 mixing ratios ($\pm 5\%$) during weekdays and weekends, which was also reported for Mexico City between 1986 and 2007 [49]. By contrast, a weekend effect in O_3 levels was observed between 2007 and 2009 within the urban areas of Oporto and Lisbon in Portugal and London, which was ascribed to changes in meteorology [9]. Within the MMA, the lowest difference between weekdays and weekends in the O_3/NO_y ratios is seen in winter, when the lowest O_3/NO_y is also observed and contrasts with the largest difference seen in summer when the highest O_3/NO_y was calculated. The higher O_3/NO_y ratios observed during summer are likely due to a combination of low NO_x emissions and meteorological conditions that foster the fast dispersion of air pollutants, limiting the presence of photochemically-processed air masses in the MMA [47].

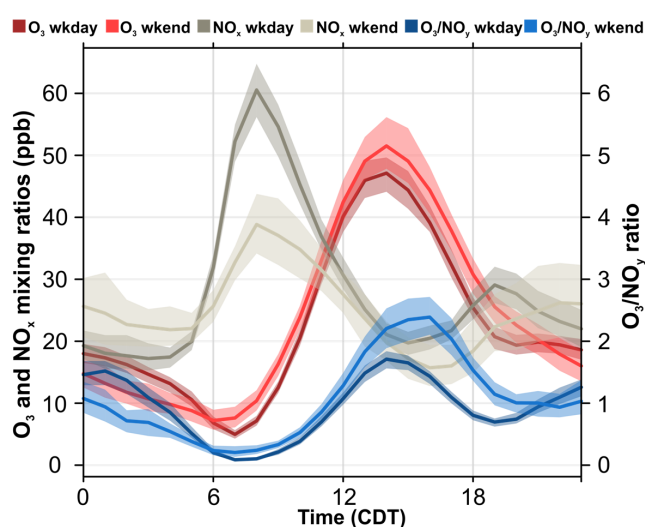


Figure 10. Average daily cycles for O_3 and NO_x mixing ratios and O_3/NO_y ratios during weekdays and weekends from September 2012 to August 2013. The shading represents the 95% confidence intervals estimated through the bootstrap resampling.

Table 6. Results of the ANOVA carried out for the average O_3/NO_y ratios calculated between 12:00 and 18:00 CDT at the OBI site during weekdays and weekends from September 2012 to August 2013.

Season	O_3/NO_y *	
	Weekdays	Weekends
Fall 2012	1.31 ± 1.07	1.81 ± 1.45
Winter 2012	1.17 ± 0.67	1.29 ± 0.85
Spring 2013	1.41 ± 1.25	1.77 ± 1.08
Summer 2013	2.13 ± 1.16	2.85 ± 1.65

* Significance level $\alpha = 0.05$.

3.5. Box Modeling

The P_{perox} was calculated by summing the production rates of H_2O_2 ($P_{H_2O_2}$), hydroperoxides and other peroxides, although $P_{H_2O_2}$ represents by far the largest contribution to P_{perox} . The P_{HNO_3} was estimated from the reaction rate of the $HO^\bullet + NO_2 \rightarrow HNO_3$ reaction. Figure 11a shows the distribution of the hourly average P_{HNO_3}/P_{perox} ratios calculated between 12:00 and 18:00 CDT for

each modeled period. The modeled P_{HNO_3}/P_{perox} ratios are consistently >2 for all selected periods, which correspond to a VOC-sensitive regime and are in good agreement with the results derived from the observational approach described here. Negative values of P_{HNO_3}/P_{perox} ratios account for 5.6% of the total data and are observed mostly between 12:00 and 13:00 CDT due to peroxide consumption at the beginning of the period of enhanced O_3 production. Figure 11b shows that the O_3/NO_y ratios calculated for the whole modelling period were consistently < 6 , which confirms the VOC-sensitive regime in O_3 production within the MMA suggested by the P_{HNO_3}/P_{perox} results.

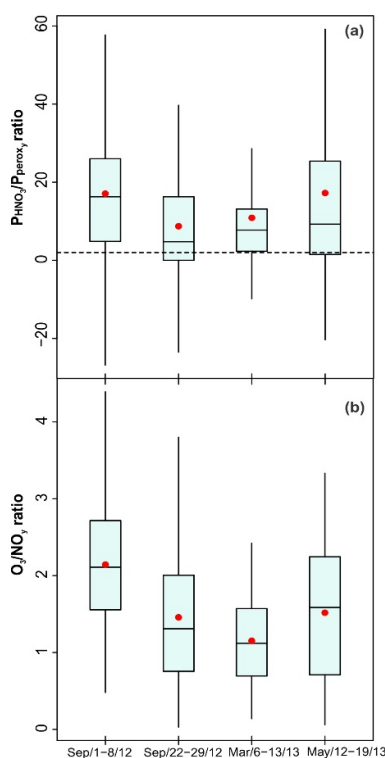


Figure 11. (a) P_{HNO_3}/P_{perox} ratios derived from box modeling for periods of O_3 mixing ratios exceeding the 110 ppb 1 h official Mexican standard in early-fall 2012 and spring 2013. Ratios greater than two, indicated by the horizontal dotted line, are typical of VOC-sensitive regimes; (b) O_3/NO_y ratios derived from observations made at the OBI site during the same periods. O_3/NO_y ratios lower than six are typically observed in VOC-sensitive regimes.

Additionally, to confirm the lack of a weekend effect in O_3 production within the MMA determined from the observational approach, an ANOVA analysis was performed to compare the modeled P_{HNO_3}/P_{perox} and O_3/NO_y ratios for weekdays and weekends of the modeled periods. Table 7 shows that no significant differences ($p > 0.05$) are observed between the average P_{HNO_3}/P_{perox} ratios during weekdays and weekends and between the average O_3/NO_y ratios during weekdays and weekends as shown in Table 6, which confirms the limiting role of VOC in production within the MMA.

Table 7. Results of the ANOVA performed for the averages of modeled P_{HNO_3}/P_{perox} ratios and O_3/NO_y ratios between 12:00 and 18:00 CDT at the OBI site during the weekdays and weekends of September 2012 and March 2013.

Period	P_{HNO_3}/P_{perox} *	O_3/NO_y *
Weekdays	13.14 ± 21.59	1.33 ± 0.78
Weekends	14.38 ± 19.52	2.01 ± 0.95

* Significance level $\alpha = 0.05$.

The O₃ sensitivity results presented here are relevant in the context of new energy-oriented projects that are under development in the northeast of Mexico, some of them located east of the MMA. Such projects include new natural gas combined-cycle power plants that are projected to start operations by late 2016, which could have an accumulated installed capacity of up to +1.3 GW. Currently, electric utilities already installed east of the MMA add up to a total capacity of +2.1 GW, all of those being natural gas combined-cycle plants. The new facilities are projected to be supplied with natural gas imported from Texas and with shale gas expected to be exploited from the Cuenca de Burgos Basin that is also located east of the MMA. The Burgos Basin represents around two-thirds of the estimated 550 trillion cubic feet of shale gas recoverable in Mexico, which is the sixth largest reservoir in the world [50]. The introduction of shale gas extraction and energy production will likely increase the regional emissions of VOCs and NO_x, impacting the photochemistry of the MMA airshed during events of enhanced regional transport [51]. Increasing NO_x levels upwind of the MMA could foster higher O₃ levels.

Finally, from the perspective of control strategies that could be put into place to help alleviate the air pollution problem that the MMA faces, it is relevant to match the results obtained here with the local emissions inventory. According to the latest comprehensive official inventory published for the MMA [37], 47% of the VOC emissions come from mobile sources and 43% from area sources; only 8% come from point sources. In contrast, the contribution of NO_x emissions is led by mobile (48%) and point (33%) sources. From a mass-basis perspective, one could argue that control strategies should target VOC emissions from mobile sources, in particular light-duty vehicles, which account for more than 70% of these emissions, and area sources. For the latter, the main contributions are from domestic use of solvents (34%), surface cleaning (13%), liquefied petroleum gas (LPG) leaks (16%), building painting activities (9%), industrial painting processes (9%) and fugitive emissions from gasoline distribution and handling in service stations (9%). However, it has to be recognized that the composition of these VOC mixtures changes from source to source, making their ozone-forming potential different. Further studies are needed to compare the reactivity of these mixtures to establish the real benefits of reducing the emissions of one source or another. If NO_x emission control strategies are explored, these should be accompanied with VOC control strategies to ensure O₃ reductions [19].

4. Conclusions

Continuous measurements of tropospheric O₃ and NO_y were made at the OBI site near the downtown MMA and used to assess the sensitivity of the O₃ production system from September 2012 to August 2013. Within the MMA, O₃ exhibits maxima in spring in response to the enhanced photolysis of NO₂, whereas the minima are observed in winter due to the reduced SR. The highest mixing ratios of O₃ were observed in easterly air masses at a WS of 5–10 km·h⁻¹, and the lowest ones were recorded in calm winds throughout the entire year. The NO_y peaks during winter and decreases during summer, which suggests that during summer, the photochemical production is oriented to O₃ rather than to NO_y. During winter, the recorded data revealed that NO and NO₂ are the major components of NO_y.

The O₃ production is enhanced between 12:00 and 18:00 CDT in line with the period of maximum SR. O₃/NO_y ratios <6 were observed during the year studied, suggesting that O₃ production within the MMA is VOC sensitive. Modeled P_{HNO_3}/P_{perox} ratios > 2 for periods of O₃ episodes in fall and spring confirm the VOC-sensitive environment within the MMA derived from the observational analysis performed. The non-significant differences observed in O₃/NO_y and in P_{HNO_3}/P_{perox} between weekdays and weekends suggest the lack of a weekend effect in O₃ production. The lack of an O₃ weekend effect within the MMA confirms the limiting role of VOCs in O₃ production during weekdays. This study demonstrates the usefulness of high-precision measurements of O₃ and NO_y to assess the O₃-VOC-NO_x system's sensitivity and to independently test the accuracy of box chemical models. The results presented here allow the wholly independent validation of current air quality policies directed to reduce tropospheric O₃ levels and, if required, the design and implementation of new ones.

Acknowledgments: This study was supported by the Mexican Council for Science and Technology (CONACYT) (Grant Number CB-2010-1-154122) and by the Tecnológico de Monterrey through its Energy and Climate Change Research Group. E. Carrillo received a scholarship from the CONACYT (Scholarship Number 342028). We appreciate SIMA's support during the field campaigns conducted in this study.

Author Contributions: Alberto Mendoza and Edson R. Carrillo-Torres conceived of and designed the experiments. Edson R. Carrillo-Torres performed the experiments. Edson R. Carrillo-Torres and Iván Y. Hernández-Paniagua analyzed the data. Edson R. Carrillo-Torres, Iván Y. Hernández-Paniagua and Alberto Mendoza contributed reagents/materials/analysis tools. Edson R. Carrillo-Torres, Iván Y. Hernández-Paniagua and Alberto Mendoza wrote the paper.

Conflicts of Interest: The authors declare no conflict of interest. The founding sponsors had no role in the design of the study; in the collection, analyses or interpretation of data; in the writing of the manuscript; nor in the decision to publish the results.

References

1. Kampa, M.; Castanas, E. Human health effects of air pollution. *Environ. Pollut.* **2008**, *151*, 362–367. [[CrossRef](#)] [[PubMed](#)]
2. Ainsworth, E.A.; Yendrek, C.R.; Sitch, S.; Collins, W.J.; Emberson, L.D. The Effects of Tropospheric Ozone on Net Primary Productivity and Implications for Climate Change. *Annu. Rev. Plant Biol.* **2012**, *63*, 637–661. [[CrossRef](#)] [[PubMed](#)]
3. Monks, P.S.; Archibald, A.T.; Colette, A.; Cooper, O.; Coyle, M.; Derwent, R.; Fowler, D.; Granier, C.; Law, K.S.; Mills, G.E.; et al. Tropospheric ozone and its precursors from the urban to the global scale from air quality to short-lived climate forcer. *Atmos. Chem. Phys.* **2015**, *15*, 8889–8973. [[CrossRef](#)]
4. National Research Council. *Rethinking the Ozone Problem in Urban and Regional Air Pollution*; The National Academies Press: Washington, DC, USA, 1991.
5. Sillman, S. The relation between ozone, NO_x and hydrocarbons in urban and polluted rural environments. *Atmos. Environ.* **1999**, *33*, 1821–1845. [[CrossRef](#)]
6. Trail, M.; Tsimpidi, A.P.; Liu, P.; Tsigaridis, K.; Rudokas, J.; Miller, P.; Nenes, A.; Hu, Y.; Russell, A.G. Sensitivity of air quality to potential future climate change and emissions in the United States and major cities. *Atmos. Environ.* **2014**, *94*, 552–563. [[CrossRef](#)]
7. Geng, F.; Tie, X.; Xu, J.; Zhou, G.; Peng, L.; Gao, W.; Tang, X.; Zhao, C. Characterizations of ozone, NO_x, and VOCs measured in Shanghai, China. *Atmos. Environ.* **2008**, *42*, 6873–6883. [[CrossRef](#)]
8. Chou, C.C.K.; Tsai, C.Y.; Chang, C.C.; Lin, P.H.; Liu, S.C.; Zhu, T. Photochemical production of ozone in Beijing during the 2008 Olympic Games. *Atmos. Chem. Phys.* **2011**, *11*, 9825–9837. [[CrossRef](#)]
9. Pires, J.C.M. Ozone Weekend Effect Analysis in Three European Urban Areas. *CLEAN—Soil Air Water* **2012**, *40*, 790–797. [[CrossRef](#)]
10. Pusede, S.E.; Cohen, R.C. On the observed response of ozone to NO_x and VOC reactivity reductions in San Joaquin Valley California 1995–present. *Atmos. Chem. Phys.* **2012**, *12*, 8323–8339. [[CrossRef](#)]
11. Wałaszek, K.; Kryza, M.; Werner, M.; Ojrzyńska, H. Sensitivity of Ground-Level Ozone to NO_x Emission During a High Ozone Episode in SW Poland. In *Air Pollution Modeling and Its Application XXIV*; Steyn, G.D., Chaumerliac, N., Eds.; Springer International Publishing: Cham, Switzerland, 2016; pp. 339–343.
12. Torres-Jardón, R.; García-Reynoso, J.A.; Jazcilevich, A.; Ruiz-Suárez, L.G.; Keener, T.C. Assessment of the Ozone-Nitrogen Oxide-Volatile Organic Compound Sensitivity of Mexico City through an Indicator-Based Approach: Measurements and Numerical Simulations Comparison. *J. Air Waste Manag. Assoc.* **2009**, *59*, 1155–1172. [[CrossRef](#)] [[PubMed](#)]
13. Cai, C.; Kelly, J.T.; Avise, J.C.; Kaduwela, A.P.; Stockwell, W.R. Photochemical Modeling in California with Two Chemical Mechanisms: Model Intercomparison and Response to Emission Reductions. *J. Air Waste Manag. Assoc.* **2011**, *61*, 559–572. [[CrossRef](#)] [[PubMed](#)]
14. Hammer, M.U.; Vogel, B.; Vogel, H. Findings on H₂O₂/HNO₃ as an indicator of ozone sensitivity in Baden-Württemberg, Berlin-Brandenburg, and the Po valley based on numerical simulations. *J. Geophys. Res.* **2002**, *107*. [[CrossRef](#)]
15. Shon, Z.H.; Lee, G.; Song, S.K.; Lee, M.; Han, J.; Lee, D. Characteristics of reactive nitrogen compounds and other relevant trace gases in the atmosphere at urban and rural areas of Korea during May–June, 2004. *J. Atmos. Chem.* **2007**, *58*, 203–218. [[CrossRef](#)]

16. Kondo, Y.; Morino, Y.; Fukuda, M.; Kanaya, Y.; Miyazaki, Y.; Takegawa, N.; Tanimoto, H.; McKenzie, R.; Johnston, P.; Blake, D.R.; et al. Formation and transport of oxidized reactive nitrogen, ozone, and secondary organic aerosol in Tokyo. *J. Geophys. Res.* **2008**, *113*. [[CrossRef](#)]
17. Chou, C.C.K.; Tsai, C.-Y.; Shiu, C.-J.; Liu, S.C.; Zhu, T. Measurement of NO_y during Campaign of Air Quality Research in Beijing 2006 (CAREBeijing-2006): Implications for the ozone production efficiency of NO_x. *J. Geophys. Res.* **2009**, *114*. [[CrossRef](#)]
18. Peng, Y.P.; Chen, K.S.; Wang, H.K.; Lai, C.H. In Situ Measurements of Hydrogen Peroxide, Nitric Acid and Reactive Nitrogen to Assess the Ozone Sensitivity in Pingtung County, Taiwan. *Aerosol Air Qual. Res.* **2011**, *11*, 59–69. [[CrossRef](#)]
19. Sierra, A.; Vanoye, A.Y.; Mendoza, A. Ozone sensitivity to its precursor emissions in northeastern Mexico for a summer air pollution episode. *J. Air Waste Manag. Assoc.* **2013**, *63*, 1221–1233. [[CrossRef](#)] [[PubMed](#)]
20. Peng, Y.P.; Chen, K.S.; Lai, C.H.; Lu, P.J.; Kao, J.H. Concentrations of H₂O₂ and HNO₃ and O₃-VOC-NO_x sensitivity in ambient air in southern Taiwan. *Atmos. Environ.* **2006**, *40*, 6741–6751. [[CrossRef](#)]
21. Castell, N.; Stein, A.F.; Mantilla, E.; Salvador, R.; Millán, M. Evaluation of the use of photochemical indicators to assess ozone—NO_x-VOC sensitivity in the Southwestern Iberian Peninsula. *J. Atmos. Chem.* **2009**, *63*, 73–91. [[CrossRef](#)]
22. Ge, B.Z.; Xu, X.B.; Lin, W.L.; Lie, J.; Wang, Z.F. Impact of the regional transport of urban Beijing pollutants on downwind areas in summer: Ozone production efficiency analysis. *Tellus B* **2012**, *64*, 17348. [[CrossRef](#)]
23. Trainer, M.; Parrish, D.D.; Buhr, M.P.; Norton, R.B.; Fehsenfeld, F.C.; Anlauf, K.G.; Bottenheim, J.W.; Tang, Y.Z.; Wiebe, H.A.; Roberts, J.M.; et al. Correlation of ozone with NO_y in photochemically aged air. *J. Geophys. Res.* **1993**, *98*, 2917–2925. [[CrossRef](#)]
24. Milford, J.B.; Gao, D.; Sillman, S.; Blosser, P.; Russell, A.G. Total reactive nitrogen (NO_y) as an indicator of the sensitivity of ozone to reductions in hydrocarbon and NO_x emissions. *J. Geophys. Res.* **1994**, *99*, 3533–3542. [[CrossRef](#)]
25. Sillman, S.; He, D. Some theoretical results concerning O₃-NO_x-VOC chemistry and NO_x-VOC indicators. *J. Geophys. Res.* **2002**, *107*. [[CrossRef](#)]
26. Miñarro, M.D.; Castell-Balaguer, N.; Téllez, L.; Mantilla, E. The use of experimental data and their uncertainty for assessing ozone photochemistry in the Eastern Iberian Peninsula. *Chemosphere* **2012**, *89*, 796–804. [[CrossRef](#)] [[PubMed](#)]
27. SEMARNAT. Informe Nacional de la Calidad del Aire 2013, Mexico. Available online: http://www.inecc.gob.mx/descargas/calaires/2014_inf_nal_calaires_mex.pdf (accessed on 20 September 2016).
28. National Institute of Information, Statistics and Geography. México en Cifras. Available online: <http://www3.inegi.org.mx/sistemas/mexicocifras/default.aspx?e=19> (accessed on 22 May 2016).
29. Servicio Meteorológico Nacional. Available online: <http://smn.cna.gob.mx/es> (accessed on 21 May 2016).
30. Carslaw, D.C.; Ropkins, K. Openair—An R package for air quality data analysis. *Environ. Model. Softw.* **2012**, *27–28*, 52–61. [[CrossRef](#)]
31. R Core Team. R: A language and Environment for Statistical Computing. Available online: <http://www.R-project.org/> (accessed on 15 February 2015).
32. Harley, R.A.; Russell, A.G.; McRae, G.J.; Cass, G.R.; Seinfeld, J.H. Photochemical modeling of the Southern California air quality study. *Environ. Sci. Technol.* **1993**, *27*, 378–388. [[CrossRef](#)]
33. Sánchez-Ccoyllo, O.R.; Ynoue, R.Y.; Martins, L.D.; de Fátima Andrade, M. Impacts of ozone precursor limitation and meteorological variables on ozone concentration in São Paulo, Brazil. *Atmos. Environ.* **2006**, *40*, 552–562. [[CrossRef](#)]
34. Ying, Q.; Lu, J.; Kleeman, M. Modeling air quality during the California Regional PM₁₀/PM_{2.5} Air Quality Study (CPRAQS) using the UCD/CIT source-oriented air quality model—Part III. Regional source apportionment of secondary and total airborne particulate matter. *Atmos. Environ.* **2009**, *43*, 419–430. [[CrossRef](#)]
35. Young, A.T.; Betterton, E.A.; De Rueda, L.S. Photochemical box model for Mexico City. *Atmósfera* **1997**, *10*, 161–178.
36. Carter, W.P.L. A detailed mechanism for the gas-phase atmospheric reactions of organic compounds. *Atmos. Environ. Part A Gen. Top.* **1990**, *24*, 481–518. [[CrossRef](#)]
37. SEMARNAT. National Emissions Inventory 2005-Inventario Nacional de Emisiones 2005 (NEI). Available online: <http://sinea.semarnat.gob.mx/sinae.php?process=UkVQT1JURUFETII=&categ=1> (accessed on 22 May 2016).

38. Mendoza, A.; García, M.R. Aplicación de un modelo de calidad del aire de segunda generación a la zona metropolitana de Guadalajara, México. *Rev. Int. Contam. Ambient.* **2009**, *25*, 73–85.
39. Hsu, Y.; Strait, R.; Roe, S.; Holoman, D. *SPECIATE 4.0 Speciation Database Development Documentation: Final Report*; EPA/6007R-06/161; US Environmental Protection Agency: Research Triangle Park, NC, USA, 2006.
40. Menchaca-Torre, H.L.; Mercado-Hernández, R.; Mendoza-Domínguez, A. Diurnal and seasonal variation of volatile organic compounds in the atmosphere of Monterrey, Mexico. *Atmos. Pollut. Res.* **2015**, *6*, 1073–1081. [[CrossRef](#)]
41. Menchaca-Torre, H.L.; Mercado-Hernández, R.; Rodríguez-Rodríguez, J.; Mendoza-Domínguez, A. Diurnal and seasonal variations of carbonyls and their effect on ozone concentrations in the atmosphere of Monterrey, Mexico. *J. Air Waste Manag. Assoc.* **2015**, *65*, 500–510. [[CrossRef](#)] [[PubMed](#)]
42. Luecken, D.J.; Tonnesen, G.S.; Sickles, I.J.E. Differences in NO_y speciation predicted by three photochemical mechanisms. *Atmos. Environ.* **1999**, *33*, 1073–1084. [[CrossRef](#)]
43. Luke, W.T.; Kelley, P.; Lefer, B.L.; Flynn, J.; Rappenglück, B.; Leuchner, M.; Dibb, J.E.; Ziemba, L.D.; Anderson, C.H.; Buhr, M. Measurements of primary trace gases and NO_y composition in Houston, Texas. *Atmos. Environ.* **2010**, *44*, 4068–4080. [[CrossRef](#)]
44. Atkinson, R. Atmospheric chemistry of VOCs and NO_x. *Atmos. Environ.* **2000**, *34*, 2063–2101. [[CrossRef](#)]
45. Cerón-Bretón, J.G.; Cerón-Bretón, R.M.; Kahl, J.D.W.; Ramírez-Lara, E.; Guarnaccia, C.; Aguilar-Ucán, C.A.; Montalvo-Romero, C.; Anguebes-Franceschi, F.; López-Chuken, U. Diurnal and seasonal variation of BTEX in the air of Monterrey, Mexico: Preliminary study of sources and photochemical ozone pollution. *Air Qual. Atmos. Health* **2015**, *8*, 469–482. [[CrossRef](#)]
46. Slowik, J.G.; Brook, J.; Chang, R.Y.W.; Evans, G.J.; Hayden, K.; Jeong, C.H.; Li, S.M.; Liggio, J.; Liu, P.S.K.; McGuire, M.; et al. Photochemical processing of organic aerosol at nearby continental sites: Contrast between urban plumes and regional aerosol. *Atmos. Chem. Phys.* **2011**, *11*, 2991–3006. [[CrossRef](#)]
47. Hernández Paniagua, I.Y.; Clemitshaw, K.C.; Mendoza, A. Impact of emissions of VOCs and NO_x on trends of ground-level O₃ in Mexico during 1993–2014: Comparison of Monterrey with Mexico City and Guadalajara. *Atmos. Chem. Phys. Discuss.* **2016**, *2016*, 1–36. [[CrossRef](#)]
48. Song, J.; Lei, W.; Bei, N.; Zavala, M.; de Foy, B.; Volkamer, R.; Cardenas, B.; Zheng, J.; Zhang, R.; Molina, L.T. Ozone response to emission changes: A modeling study during the MCMA-2006/MILAGRO Campaign. *Atmos. Chem. Phys.* **2010**, *10*, 3827–3846. [[CrossRef](#)]
49. Stephens, S.; Madronich, S.; Wu, F.; Olson, J.B.; Ramos, R.; Retama, A.; Muñoz, R. Weekly patterns of México City's surface concentrations of CO, NO_x, PM₁₀ and O₃ during 1986–2007. *Atmos. Chem. Phys.* **2008**, *8*, 5313–5325. [[CrossRef](#)]
50. US Energy Information Administration. *Technically Recoverable Shale Oil and Shale Gas. Resources: Mexico*; United States Department of Energy: Washington, DC, USA, 2015.
51. Pacsi, A.P.; Kimura, Y.; McGaughey, G.; McDonald-Buller, E.C.; Allen, D.T. Regional Ozone Impacts of Increased Natural Gas Use in the Texas Power Sector and Development in the Eagle Ford Shale. *Environ. Sci. Technol.* **2015**, *49*, 3966–3973. [[CrossRef](#)] [[PubMed](#)]

